JAM CM Journal of Applied Mathematics and Computational Mechanics 2024, 23(2), 117-128
www.amcm.pcz.pl p-ISSN 2299-9965
DOI: 10.17512/jamcm.2024.2.10 e-ISSN 2353-0588

NUMERICAL MODELING OF THE CASTING SOLIDIFICATION PROCESS IN A MOLD TAKING INTO ACCOUNT THE INFLUENCE OF AN AIR GAP WITH VARIABLE WIDTH

Ewa Węgrzyn-Skrzypczak[1], Tomasz Skrzypczak[2]

[1] Department of Mathematics, Czestochowa University of Technology
Czestochowa, Poland
[2] Department of Mechanics and Fundamentals of Machine Design
Czestochowa University of Technology
Czestochowa, Poland
ewa.wegrzyn-skrzypczak@pcz.pl, tomasz.skrzypczak@pcz.pl

Received: 28 January 2024; Accepted: 4 April 2024

Abstract. The article presents a numerical modeling approach that utilizes the Finite Element Method (FEM) to simulate the solidification process of a casting in a mold. The study takes into account the local width of the air gap at each computational point on the interface between the casting and the mold. The developed numerical model provides a detailed understanding of the heat transfer between the casting and the mold during the solidification. The study shows that the air gap with variable width has a significant impact on the solidification process, affecting the cooling rate and the formation of the solidified region.

MSC 2010: *65M60, 68U20*
Keywords: *numerical modeling, finite element method, solidification, air gap width, heat transfer*

1. Introduction

Numerical modeling with the use of FEM and computer simulations of various physical processes play a crucial role in a wide variety of industrial branches. Theoretical investigations into temperature, displacements, or stress distribution in manufactured elements and tools are an essential part of numerical modeling of various processes and physical phenomena, such as the drawing of wires [1], structural behavior of sandwich panels [2, 3] or metal casting. The casting solidification process is a complex phenomenon that involves heat transfer, fluid flow and phase change of liquid metal. The quality of castings depends largely on how well the solidification process is controlled and optimized. One of the factors that affects the solidification process is the air gap that forms between the mold and the casting due to shrinkage of metal during cooling. The air gap acts as a thermal resistance

that reduces the heat transfer rate from the casting to the mold, thus prolonging the solidification time and increasing the risk of defects such as porosity, hot tearing and segregation. Numerical modeling is a useful tool to study and predict the solidification process taking into account the influence of the air gap with variable width. Numerical models are built on the foundation of coupled equations governing mass, momentum, energy, and species conservation for both liquid and solid phases. They also incorporate methods for tracking the solid-liquid interface and calculating air gap width. Different boundary conditions describing mold cooling, electromagnetic stirring, or water immersion are used to simulate different casting scenarios. Mortensen et al. [4] coupled modeling of air-gap formation and surface exudation during the casting of aluminium extrusion ingots. They found that the surface pull-in force magnifies the air-gap during solidification close to the mold surface. They also studied how the surface exudation affects heat transfer and microstructure formation. The paper [5] studied heat transfer on the solidification of the casting process with different mold materials. The authors found that mold material properties affect heat transfer coefficient, cooling rate and solidification time. They also discussed how the air gap formation influences a heat transfer between the casting and the mold. Li et al. [6] measured the air gap formation during steel-ingot casting and its effect on interfacial heat transfer. They found that the air gap forms earlier and grows larger on the narrow side than on the width side of the ingot. They also proposed a simple equation to predict IHTC based on conduction, radiation and contact resistance across the gap. Xu et al. [7] simulated the directional solidification process with the multi-shell mold being gradually immersed in water after pouring. They found that this method can enhance heat transfer by reducing air gap formation and achieve fine grains and superior mechanical properties for castings. Chawla et al. [8] modeled solidification process taking into account metal--mold air gaps for the horizontal continuous casting of cast iron. They found that air gap length and thickness have a substantial effect on solid and eutectic area at the top-outlet end of the die. They also aimed to optimize process parameters for shell thickness control.

The presented work takes into account that the rate of the solidification process is influenced by the variable size of the air gap between the casting and the mold, which is directly incorporated into the model. To achieve this, FEM was employed with separate spatial discretization for both the mold and the casting. The thermally dependent changes in their volumes were considered, taking into account resulting displacements. To obtain temporary temperature fields, the approach involved the use of two separate meshes. The appropriate boundary condition describes the thermal interaction between the mold and the casting, and the solution is independently obtained for each region in each time step using an iterative procedure. A novel element of the presented work, compared to the literature, is the method of calculating the air gap. During the deformations of the casting and the mold, the width of the gap between them is calculated at each time step as the local distance between surfaces in thermal contact. A similar approach was presented in [9], but in the case of a two-dimensional problem.

2. Mathematical model

Figure 1 provides a schematic representation of the problem at hand, which involves the entire region being divided into two volumes. The first volume, represented by Ω_M, is the cast iron mold, while the second part, Ω_C, comprises the solidifying steel that fills the mold. As the alloy undergoes a liquid-solid transition, the heat of solidification is released, leading to thermal deformations in both the mold and the casting. A gap appears between the internal fragments of boundaries Γ_M and Γ_C, except at the local bottom area, where there is almost perfect contact. This gap's local width, h, changes as the temperatures of the mold and casting evolve. Heat transfer occurs from the casting to the mold through the forming gap, but its intensity is significantly affected by the increase in thermal resistance. The ambient temperature being lower than the mold and casting temperatures means that heat is also transported outside through the external surfaces of the mold-casting system. Additionally, air is present in the gap between the mold and casting, which can affect the heat transport characteristics. Neglected factors in the model include gravity forces, mechanical loads, and shrinkage during the liquid-solid phase change.

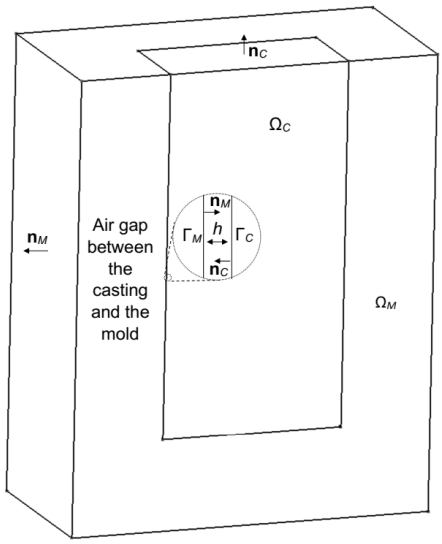

Fig. 1. Mold and casting with a gap between them

In order to describe the behavior of the presented mold-casting system, the following equations are used as its governing equations:
The heat conduction equation is used to describe the transient heat transfer in a three--dimensional volume:

$$\frac{\partial}{\partial x}\left(\lambda_{(i)}\frac{\partial T^{(i)}}{\partial x}\right)+\frac{\partial}{\partial y}\left(\lambda_{(i)}\frac{\partial T^{(i)}}{\partial y}\right)+\frac{\partial}{\partial z}\left(\lambda_{(i)}\frac{\partial T^{(i)}}{\partial z}\right)=c_{(i)}\rho_{(i)}\frac{\partial T^{(i)}}{\partial t} \tag{1}$$

The equations of static equilibrium:

$$\begin{aligned}
\frac{\partial \sigma_x^{(i)}}{\partial x}+\frac{\partial \tau_{xy}^{(i)}}{\partial y}+\frac{\partial \tau_{xz}^{(i)}}{\partial z}&=0\\
\frac{\partial \tau_{xy}^{(i)}}{\partial x}+\frac{\partial \sigma_y^{(i)}}{\partial y}+\frac{\partial \tau_{yz}^{(i)}}{\partial z}&=0\\
\frac{\partial \tau_{xz}^{(i)}}{\partial x}+\frac{\partial \tau_{yz}^{(i)}}{\partial y}+\frac{\partial \sigma_z^{(i)}}{\partial z}&=0
\end{aligned} \tag{2}$$

The variables utilized in the presented model are as follows: the coefficient of thermal conductivity λ [J s^{-1} m^{-1} K^{-1}], heat capacity c [J K^{-1} kg^{-1}], density ρ [kg m^{-3}], temperature T [K], the components of symmetrical stress tensor σ_x, σ_y, σ_z, τ_{xy}, τ_{xz}, τ_{yz} [N m^{-2}], time t [s], Cartesian coordinates x, y, z [m], and the index i denoting the i-th volume. It should be noted that in this description, the index i is specifically related to either the casting (C) or the mold (M). The initial and boundary conditions for Eq. (1) are as follows:

$$T^{(C)}\left(x,y,z,0\right)=T_0^{(C)},\ T^{(M)}\left(x,y,z,0\right)=T_0^{(M)} \tag{3}$$

$$-\lambda_C\frac{\partial T^{(C)}}{\partial n_C}=\frac{\lambda_g}{h}\left(T_b^{(C)}-T_b^{(M)}\right)=\lambda_M\frac{\partial T^{(M)}}{\partial n_M} \tag{4}$$

$$-\lambda_C\frac{\partial T^{(C)}}{\partial n_C}=\alpha_C\left(T^{(C)}-T_{amb}^{(C)}\right),\ -\lambda_M\frac{\partial T^{(M)}}{\partial n_M}=\alpha_M\left(T^{(M)}-T_{amb}^{(M)}\right) \tag{5}$$

The local width of the gap is denoted by h [m], and the local directions of the vectors normal to the boundaries Γ_C and Γ_M are represented by n_C and n_M, respectively. $T_b^{(C)}$ and $T_b^{(M)}$ [K] signify the local temperatures of the volumes Ω_C and Ω_M at the contact boundaries, while $T_0^{(C)}$ and $T_0^{(M)}$ [K] are the initial temperatures of the volumes Ω_C and Ω_M, respectively. $T^{(C)}$ and $T^{(M)}$ [K] represent the local temperatures of the volumes Ω_C and Ω_M at the external boundaries. $T_{amb}^{(C)}$ and $T_{amb}^{(M)}$ [K] are the ambient temperatures outside the casting and the mold while α_C and α_M [J s^{-1} m^{-2} K^{-1}] represent heat convection coefficient at the external boundaries. Finally, the thermal conductivity of the medium filling the gap is denoted by λ_g.

The calculation of the heat capacity in the casting can be performed using the following relations [10]:

$$c_C=\begin{Bmatrix} c_s & ,T^{(C)}<T_S\\ 0.5\left(c_s+c_l\right)+\dfrac{L}{T_L-T_S} & ,T_S\le T^{(C)}\le T_L\\ c_l & ,T^{(C)}>T_L \end{Bmatrix} \tag{6}$$

where T_S and T_L [K] denote the solidus and liquidus temperatures, respectively, while c_s and c_l [J kg^{-1} K^{-1}] indicate the specific heat capacities of the solid and liquid phases of the casting. L [J kg^{-1}] represents the latent heat of solidification.

The equations (2) contain six unknowns, which can be transformed into displacement-dependent functions. To achieve this, the following relations are utilized:

$$\begin{aligned}
\sigma_x^{(i)} &= \frac{E_{(i)}}{1+\nu_{(i)}}\left[\varepsilon_x^{(i)} + \frac{\nu_{(i)}}{1-2\nu_{(i)}}\left(\varepsilon_x^{(i)}+\varepsilon_y^{(i)}+\varepsilon_z^{(i)}\right) - \frac{1+\nu_{(i)}}{1-2\nu_{(i)}}a_{(i)}\Delta T^{(i)}\right] \\
\sigma_y^{(i)} &= \frac{E_{(i)}}{1+\nu_{(i)}}\left[\varepsilon_y^{(i)} + \frac{\nu_{(i)}}{1-2\nu_{(i)}}\left(\varepsilon_x^{(i)}+\varepsilon_y^{(i)}+\varepsilon_z^{(i)}\right) - \frac{1+\nu_{(i)}}{1-2\nu_{(i)}}a_{(i)}\Delta T^{(i)}\right] \\
\sigma_z^{(i)} &= \frac{E_{(i)}}{1+\nu_{(i)}}\left[\varepsilon_z^{(i)} + \frac{\nu_{(i)}}{1-2\nu_{(i)}}\left(\varepsilon_x^{(i)}+\varepsilon_y^{(i)}+\varepsilon_z^{(i)}\right) - \frac{1+\nu_{(i)}}{1-2\nu_{(i)}}a_{(i)}\Delta T^{(i)}\right] \\
\tau_{xy}^{(i)} &= \frac{E_{(i)}}{2\left(1+\nu_{(i)}\right)}\gamma_{xy}^{(i)} \\
\tau_{yz}^{(i)} &= \frac{E}{2\left(1+\nu_{(i)}\right)}\gamma_{yz}^{(i)} \\
\tau_{xz}^{(i)} &= \frac{E}{2\left(1+\nu_{(i)}\right)}\gamma_{xz}^{(i)}
\end{aligned} \tag{7}$$

$$\begin{aligned}
\varepsilon_x^{(i)} &= \frac{\partial u_x^{(i)}}{\partial x},\ \gamma_{xy}^{(i)} = \frac{\partial u_x^{(i)}}{\partial y} + \frac{\partial u_y^{(i)}}{\partial x} \\
\varepsilon_y^{(i)} &= \frac{\partial u_y^{(i)}}{\partial y},\ \gamma_{yz}^{(i)} = \frac{\partial u_y^{(i)}}{\partial z} + \frac{\partial u_z^{(i)}}{\partial y} \\
\varepsilon_z^{(i)} &= \frac{\partial u_z^{(i)}}{\partial z},\ \gamma_{xz}^{(i)} = \frac{\partial u_x^{(i)}}{\partial z} + \frac{\partial u_z^{(i)}}{\partial x}
\end{aligned} \tag{8}$$

The components of the symmetrical strain tensor are represented by ε_x, ε_y, ε_z, γ_{xy}, γ_{xz}, and γ_{yz} [–]. Meanwhile, the components of the displacement vector are denoted by u_x, u_y, and u_z [m]. Other variables used in the above equations include E [N m^{-2}] for Young's modulus, ν [–] for Poisson's ratio, a [K^{-1}] for the linear thermal expansion coefficient, and ΔT [K] for the temperature difference between the reference and current states, which is given by $\Delta T = T - T_{ref}$.

After utilizing relations (8) in equations (7) and subsequently inserting the stress components into the equilibrium equations (2), the resulting equations are as follows:

$$
\begin{aligned}
&f_1\frac{\partial^2 u_x^{(i)}}{\partial x^2}+f_2\left(\frac{\partial^2 u_y^{(i)}}{\partial x\partial y}+\frac{\partial^2 u_z^{(i)}}{\partial x\partial z}\right)+f_3\left(\frac{\partial^2 u_x^{(i)}}{\partial y^2}+\frac{\partial^2 u_x^{(i)}}{\partial z^2}+\frac{\partial^2 u_y^{(i)}}{\partial y\partial x}+\frac{\partial^2 u_z^{(i)}}{\partial z\partial x}\right)+f_4 a_{(i)}\Delta T^{(i)}=0\\
&f_1\frac{\partial^2 u_y^{(i)}}{\partial y^2}+f_2\left(\frac{\partial^2 u_x^{(i)}}{\partial y\partial x}+\frac{\partial^2 u_z^{(i)}}{\partial y\partial z}\right)+f_3\left(\frac{\partial^2 u_x^{(i)}}{\partial x\partial y}+\frac{\partial^2 u_y^{(i)}}{\partial x^2}+\frac{\partial^2 u_y^{(i)}}{\partial z^2}+\frac{\partial^2 u_z^{(i)}}{\partial z\partial y}\right)+f_4 a_{(i)}\Delta T^{(i)}=0\\
&f_1\frac{\partial^2 u_z^{(i)}}{\partial z^2}+f_2\left(\frac{\partial^2 u_x^{(i)}}{\partial z\partial x}+\frac{\partial^2 u_y^{(i)}}{\partial z\partial y}\right)+f_3\left(\frac{\partial^2 u_x^{(i)}}{\partial x\partial z}+\frac{\partial^2 u_y^{(i)}}{\partial y\partial z}+\frac{\partial^2 u_z^{(i)}}{\partial x^2}+\frac{\partial^2 u_z^{(i)}}{\partial y^2}\right)+f_4 a_{(i)}\Delta T^{(i)}=0
\end{aligned}
\tag{9}
$$

The definitions of f_1, f_2, f_3, and f_4 are provided below:

$$
\begin{aligned}
f_1&=\frac{E_{(i)}\left(1-\nu_{(i)}\right)}{\left(1+\nu_{(i)}\right)\left(1-2\nu_{(i)}\right)},\quad f_2=\frac{E_{(i)}\nu_{(i)}}{\left(1+\nu_{(i)}\right)\left(1-2\nu_{(i)}\right)}\\
f_3&=\frac{E_{(i)}}{2\left(1+\nu_{(i)}\right)},\quad f_4=\frac{E_{(i)}\left(1+\nu_{(i)}\right)}{\left(1+\nu_{(i)}\right)\left(1-2\nu_{(i)}\right)}
\end{aligned}
\tag{10}
$$

Equations (9) must be supplemented by the appropriate boundary conditions defining known displacements at chosen surfaces (most often on the planes of symmetry) or in the particular point of the casting and the mold.

3. Numerical model

The finite element method (FEM) serves as the foundation for the numerical model presented in this study. This model is derived from the method of weighted residuals. To obtain the weak form of equations (1) and (9), both equations are multiplied by the weighting function w and integrated over the volume Ω_i. The resulting weak form is as follows:

$$
\int_{\Omega_i}\lambda_{(i)}\left(\frac{\partial w}{\partial x}\frac{\partial T^{(i)}}{\partial x}+\frac{\partial w}{\partial y}\frac{\partial T^{(i)}}{\partial y}+\frac{\partial w}{\partial z}\frac{\partial T^{(i)}}{\partial z}\right)d\Omega_i+\int_{\Omega_i}c_{(i)}\rho_{(i)}w\frac{\partial T^{(i)}}{\partial t}d\Omega_i=\int_{\Gamma_i}wqd\Gamma_i \tag{11}
$$

$$
\begin{aligned}
&\int_{\Omega_i}\left(f_1\frac{\partial w}{\partial x}\frac{\partial u_x^{(i)}}{\partial x}+f_3\frac{\partial w}{\partial y}\frac{\partial u_x^{(i)}}{\partial y}+f_3\frac{\partial w}{\partial z}\frac{\partial u_x^{(i)}}{\partial z}\right)d\Omega_i+\\
&+\int_{\Omega_i}\left(f_2\frac{\partial w}{\partial x}\frac{\partial u_y^{(i)}}{\partial y}+f_3\frac{\partial w}{\partial y}\frac{\partial u_y^{(i)}}{\partial x}\right)d\Omega_i+\\
&+\int_{\Omega_i}\left(f_2\frac{\partial w}{\partial x}\frac{\partial u_z^{(i)}}{\partial z}+f_3\frac{\partial w}{\partial z}\frac{\partial u_z^{(i)}}{\partial x}\right)d\Omega_i=\int_{\Gamma_i}f_4 a_{(i)}\frac{\partial w}{\partial x}\Delta T^{(i)}d\Gamma_i
\end{aligned}
\tag{12}
$$

$$\int_{\Omega_i}\left(f_2\frac{\partial w}{\partial y}\frac{\partial u_x^{(i)}}{\partial x}+f_3\frac{\partial w}{\partial x}\frac{\partial u_x^{(i)}}{\partial y}\right)d\Omega_i+$$
$$+\int_{\Omega_i}\left(f_3\frac{\partial w}{\partial x}\frac{\partial u_y^{(i)}}{\partial x}+f_1\frac{\partial w}{\partial y}\frac{\partial u_y^{(i)}}{\partial y}+f_3\frac{\partial w}{\partial z}\frac{\partial u_y^{(i)}}{\partial z}\right)d\Omega_i+ \tag{13}$$
$$+\int_{\Omega_i}\left(f_2\frac{\partial w}{\partial y}\frac{\partial u_z^{(i)}}{\partial z}+f_3\frac{\partial w}{\partial z}\frac{\partial u_z^{(i)}}{\partial y}\right)d\Omega_i=\int_{\Gamma_i}f_4 a_{(i)}\frac{\partial w}{\partial y}\Delta T^{(i)}d\Gamma_i$$

$$\int_{\Omega_i}\left(f_2\frac{\partial w}{\partial z}\frac{\partial u_x^{(i)}}{\partial x}+f_3\frac{\partial w}{\partial x}\frac{\partial u_x^{(i)}}{\partial z}\right)d\Omega_i+\int_{\Omega_i}\left(f_2\frac{\partial w}{\partial z}\frac{\partial u_y^{(i)}}{\partial y}+f_3\frac{\partial w}{\partial y}\frac{\partial u_y^{(i)}}{\partial z}\right)d\Omega_i+$$
$$+\int_{\Omega_i}\left(f_3\frac{\partial w}{\partial x}\frac{\partial u_z^{(i)}}{\partial x}+f_3\frac{\partial w}{\partial y}\frac{\partial u_z^{(i)}}{\partial y}+f_1\frac{\partial w}{\partial z}\frac{\partial u_z^{(i)}}{\partial z}\right)d\Omega_i=\int_{\Gamma_i}f_4 a_{(i)}\frac{\partial w}{\partial z}\Delta T^{(i)}d\Gamma_i \tag{14}$$

The Galerkin method asserts that the weighting functions, denoted as w, are the same as the shape functions employed in the meshing process for finite elements. The discretization of equation (11) with respect to time follows the implicit Euler method. The final expression for the comprehensive FEM equations is outlined as follows:

$$\mathbf{K}_T^{(i)}\mathbf{T}_{f+1}^{(i)}+\mathbf{M}_T^{(i)}\frac{\mathbf{T}_{f+1}^{(i)}-\mathbf{T}_f^{(i)}}{\Delta t}=\mathbf{B}_T^{(i)} \tag{15}$$

$$\mathbf{K}_D^{(i)}\mathbf{u}^{(i)}=\mathbf{B}_D^{(i)} \tag{16}$$

where $\mathbf{K}_T$ represents the comprehensive thermal conductivity matrix at a global scale, while $\mathbf{M}_T$ stands for the global thermal capacity matrix. The vector $\mathbf{B}_T$ corresponds to the global vector linked to thermal boundary conditions, and $\mathbf{T}$ denotes the vector encompassing unknown nodal temperatures at a particular time level, represented by f. Additionally, $\mathbf{K}_D$ signifies the global stiffness matrix, $\mathbf{B}_D$ is a vector housing known boundary displacements, and $\mathbf{u}$ stands for the vector containing unknown nodal displacements.

At each step, the iterative process independently obtains the solution for equation (15) in each region. The determined temperatures are subsequently employed to calculate the thermal deformations in the casting and in the mold using (16). It is important to use the condition (4) during the solution process of the heat transport equation [11]. Throughout the deformations of Ω_C and Ω_M, the mutual positions of the casting and the mold as well as the width of the gap change according to time. The approach presented relies on disconnected finite element meshes, as the global set of equations is constructed and solved independently for each region.

4. Example of calculations

The original computer program was created to simulate the described process. Table 1 outlines the material properties of both the casting and the mold.

Table 1. Material properties used in the simulation

Material property	Casting		Mold	Air gap
	Liquid phase	Solid phase		
λ [J s^{-1} m^{-1} K^{-1}]	23	35	59	0.5
c [J K^{-1} kg^{-1}]	837	644	502	–
ρ [kg m^{-3}]	6915	7800	7200	–
E [N m^{-2}]	–	$2.1 \cdot 10^{11}$	$2.1 \cdot 10^{11}$	–
ν [–]	–	0.28	0.28	–
a [K^{-1}]	–	$1.2 \cdot 10^{-5}$	$1.2 \cdot 10^{-5}$	–
T_L [K]	1766		–	–
T_S [K]	1701		–	–
L [J kg^{-1}]	$2.7 \cdot 10^5$		–	–

The mold is a rectangular prism with dimensions of 0.2x0.2x0.25 m, while the casting is a cylinder with a base radius of 0.05 m and a height of 0.2 m. The mold is initially at a temperature of 600 K, and molten steel with an initial temperature of 1800 K is introduced. The pouring process and the movement of the liquid metal are neglected. Considering symmetry, only a quarter of the casting-mold system is analyzed (Fig. 2), with thermal insulation assumed on the xy and yz planes of symmetry. It is also important to introduce displacement $z = 0$ on the xy plane of symmetry and $x = 0$ on the yz plane as well as $x = y = z = 0$ at the fixed point A. Convective heat transfer is specified on the external boundaries of the mold and on the top of the casting, with a heat transfer coefficient $\alpha = 100$ J s^{-1} m^{-2} K^{-1} and an ambient temperature T_∞ of 300 K. The time step remains constant at $\Delta t = 0.1$ s. In each time step, the gas gap between the casting and the mold, characterized by a variable width and a heat conductivity $\lambda_g = 0.5$ J s^{-1} m^{-1} K^{-1}, is calculated. The geometries and meshes are generated using the GMSH preprocessor [12], employing tetrahedrons. The casting mesh comprises 6674 nodes, while the mold mesh includes 28801 nodes.

In Figures 3a-c, temperature distributions in the casting-mold system are presented at selected moments. Heat transfer primarily occurs through the expanding gas gap at the interface of the casting and the mold, and to a much lesser extent through heat dissipation from the system to the surroundings. Figures 4a-c present successive stages of solid phase growth in the casting until complete solidification

(Fig. 4c). It is worth mentioning that the rate of solid phase growth is significantly affected by the heat transport reduction due to the widening of the gas gap. Due to the rapid heat absorption by the mold, a significantly reduced solid-liquid zone is observed (Figs. 4a-b). Deformations of the casting and the mold due to cooling are illustrated in Figures 5a-c (magnified 10 times for better visualization). A noticeable reduction in the vertical dimension of the casting and gradual widening of the gas gap are apparent. After 130 seconds, when the solidification process ends (Fig. 5c), the gap width reaches 0.6 mm at the lower part of the mold-casting system, while the reduction in the vertical dimension of the casting is approximately 1.6 mm.

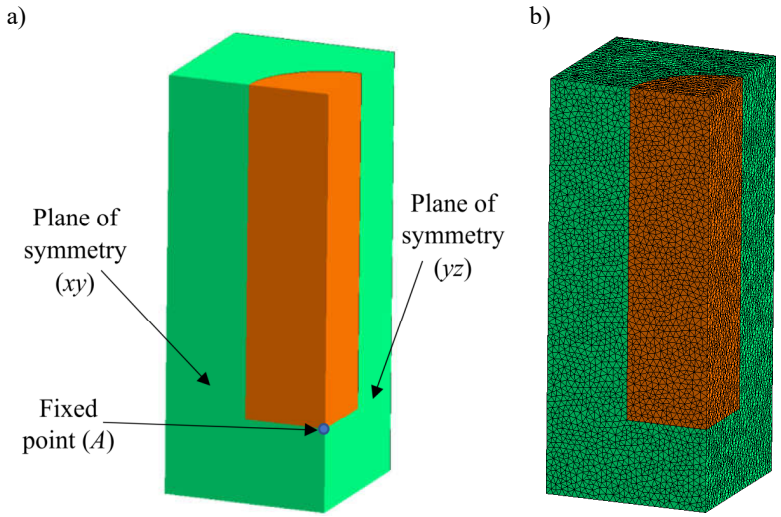

Fig. 2. Quarter of the casting-mold system (a), finite element meshes composed of tetrahedrons (b)

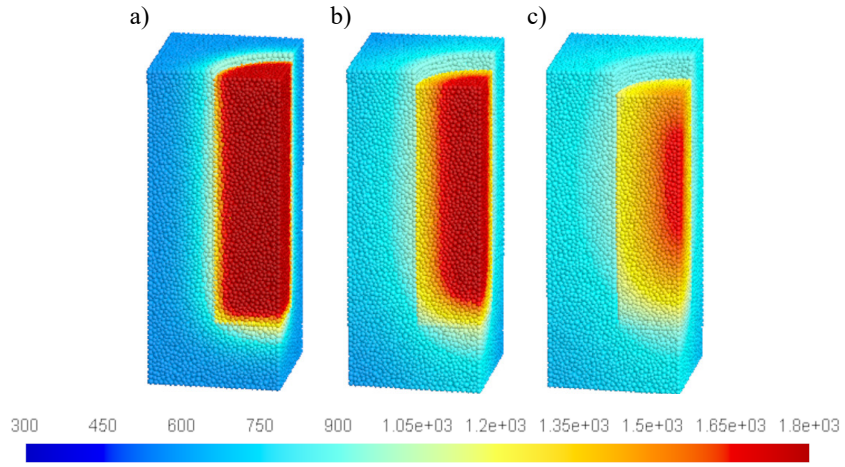

Fig. 3. Temperature distribution in the casting-mold system at t = 10 s (a), t = 60 s (b), t = 130 s (c)

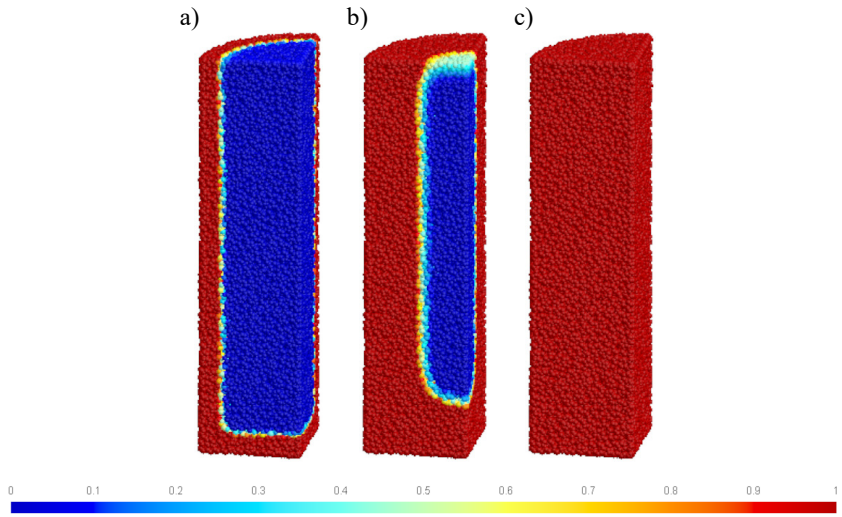

Fig. 4. Distribution of the solid phase fraction in the casting at t = 10 s (a), t = 60 s (b), t = 130 s (c)

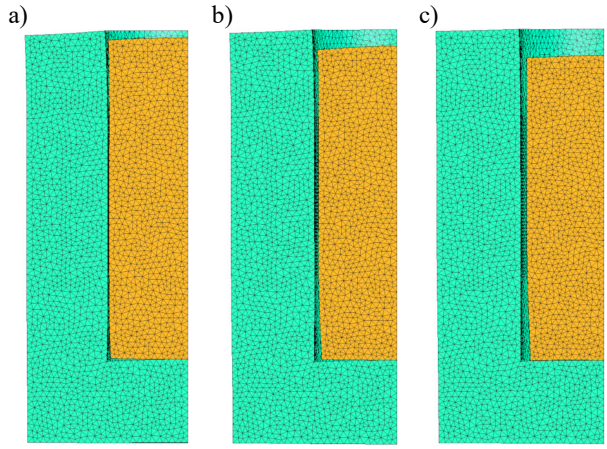

Fig. 5. Deformations of the casting-mold system (magnified 10x) at t = 10 s (a), t = 60 s (b), t = 130 s (c)

Assuming that the thermal processes in the casting and the mold are homogeneous, one can also analytically estimate the width of forming gap h [m] depending on the diameter D [m] of the casting using the following simple formula [13]:

$$h = \left[a_C \left(T_S - T_C \right) + a_M \left(T_M - T_{M0} \right) \right] D \tag{17}$$

where a_C, a_M [K^{-1}] are the coefficients of thermal expansion of the casting and the mold respectively, T_S [K] is the solidus temperature, T_C, T_M [K] represents

the temperature of the casting and the mold interface, and T_{M0} [K] is the initial temperature of the mold.

Using (17) the air gap width at the lower part of the mold-casting interface can be calculated at the end of solidification (130 s) as:

$$h = \left[1.2 \cdot 10^{-5}\left(1701 - 1250\right) + 1.2 \cdot 10^{-5}\left(675 - 600\right)\right]0.1 = 6.31 \cdot 10^{-4}$$

The above value of $h = 0.631$ mm calculated analytically has an acceptable agreement with the air gap width measured using deformed finite element meshes (0.6 mm).

5. Conclusions

The showcased mathematical and numerical models of solidification, along with the calculation outcomes, underscore the significance of considering the impact of the gas gap on the cooling dynamics of the casting. The proposed methodology, utilizing separate meshes for the mold and the casting, enables substantial operational memory savings by sequentially solving the global set of equations. Further efforts will concentrate on incorporating the mechanical interaction of thermally deformed regions into the model, as well as accounting for radiation effects within the gap. Accurately predicting the location and width of the gap becomes crucial, particularly when the casting exhibits complex external boundaries.

References

[1] Suliga, M., Szota, P., & Mróz, S. (2017). Simulation and measurement of temperature in high speed drawing process of steel wires. *Computer Methods in Materials Science*, *17*(1), 69-75. DOI: 10.7494/cmms.2017.1.0577.

[2] Pozorska, J. (2018). Numerical modelling of sandwich panels with a non-continuous soft core. *MATEC Web of Conferences*, *157*, 06007. DOI: 10.1051/matecconf/201815706007.

[3] Pozorska J., Pozorski Z., & Janik L. (2017). Numerical simulations of structural behavior of sandwich panels subjected to concentrated static loads. *Journal of Applied Mathematics and Computational Mechanics*, *16*(2), 113-121. DOI: 10.17512/jamcm.2017.2.09.

[4] Mortensen, D., Henriksen, B.R., M'Hamdi, M., & Fjær, H.G. (2016). Coupled modelling of air-gap formation and surface exudation during extrusion ingot DC-casting. In: Grandfield, J.F., Eskin, D.G. (eds). *Essential Readings in Light Metals*. Cham: Springer. DOI: 10.1007/978-3-319-48228-6_101.

[5] Gowsalya, L.A., & Afshan, M.E. (2021). Heat transfer studies on solidification of casting process. in: *Casting Processes and Modelling of Metallic Materials*. DOI: 10.5772/intechopen.95371.

[6] Li, W., Li, L., Geng, Y., Zang, X., Jing, Y., Li, D., & Thomas, B.G. (2021). Air gap measurement during steel-ingot casting and its effect on interfacial heat transfer. *Metallurgical and Materials Transactions B*, *52*, 2224-2238. DOI: 10.1007/s11663-021-02152-3.

[7] Xu, J., Kang, J., Zheng, L., Mao, W., & Wang, J. (2022). Numerical simulation of the directional solidification process with multi-shell mold being gradually immersed in water. *Journal of Materials Research and Technology*, *19*, 2705-2716. DOI: 10.1016/j.jmrt.2022.06.037.

[8] Chawla, A., Tiedje, N.S., & Spangenberg, J. (2023). Numerical modelling for the effect of metal--mould air gaps on shell thickness in horizontal continuous casting of cast iron. *Archives of Foundry Engineering*, *23*(1), 8 p. DOI: 10.24425/afe.2023.144280.

[9] Skrzypczak, T., Węgrzyn-Skrzypczak, E., & Sowa, L. (2018). Numerical modeling of solidification process taking into account the effect of air gap. *Applied Mathematics and Computation*, *321*, 768-779. DOI: 10.1016/j.amc.2017.11.023.

[10] Mochnacki, B., & Suchy. J.S. (1993). *Modeling and Simulation of Solidification of Castings*. Warsaw: PWN.

[11] Skrzypczak T., & Węgrzyn-Skrzypczak, E. (2015). Modeling of thermal contact through gap with the use of finite element method, *Journal of Applied Mathematics and Computational Mechanics*, *14*(4), 145-152. DOI: 10.17512/jamcm.2015.4.15.

[12] Geuzaine, C., & Remacle, J.-F. (2009). Gmsh: a three-dimensional finite element mesh generator with built-in pre- and post-processing facilities. *International Journal for Numerical Methods in Engineering*, *79*(11), 1309-1331.

[13] Campbell J. (2011). *Complete Casting Handbook – Metal Casting Processes, Techniques and Design*. Butterworth-Heinemann.